A 60-GHz Uniplanar MMIC 4× Subharmonic Mixer

Michael W. Chapman, *Member, IEEE,* and Sanjay Raman, *Member, IEEE*

***Abstract*—A uniplanar GaAs monolithic microwave integrated circuit ×4 subharmonic mixer (SHM) has been fabricated for 60-GHz-band applications using an antiparallel diode pair in finite ground coplanar (FGC) waveguide technology. This mixer is designed to operate at an RF of 58.5–60.5 GHz, an IF of 1.5–2.5 GHz, and an LO frequency of 14–14.5 GHz. FGC transmission-line structures used in the mixer implementation were fully characterized using full-wave electromagnetic simulations and on-wafer measurements. Of several mixer configurations tested, the best results show a maximum conversion loss of 13.2 dB over the specified frequency range with a minimum local-oscillator power of 3 dBm. The minimum upper sideband conversion loss is 11.3 dB at an RF of 58.5 GHz and an IF of 2.5 GHz. This represents excellent performance for a 4× SHM operating at 60 GHz.**

***Index Terms*—Coplanar transmission lines, coplanar waveguides (CPWs), millimeter-wave integrated circuits, mixers, monolithic microwave integrated circuits (MMICs), Schottky diodes.**

I. Introduction

As THE demand for high-speed high-capacity wireless data transmission becomes greater and greater, millimeter-wave frequencies, such as those in the 60-GHz band, may offer an attractive alternative to the microwave frequencies currently allocated for wireless data transmission. In particular, the 58–62-GHz frequency range has received recent attention as a possible candidate for secure high-speed wireless networks. Although an atmospheric attenuation peak exists from 58–62 GHz due to oxygen resonance, this band could be useful for short-range links in systems such as indoor wireless local area networks (WLANs) and intelligent transportation systems (ITSs) [1].

Downconverting a received signal from high frequencies such as 60 GHz presents a significant challenge to the RF circuit designer. In particular, local oscillators (LOs) with adequate output power at millimeter-wave frequencies often incorporate physically large and expensive waveguide resonators. Subharmonic mixing offers an alternative to using a higher frequency (millimeter-wave) LO. For fundamental mixers, the oscillator is separated in frequency from the RF signal by some relatively small offset equal to the IF ($f_{\mathrm{IF}} = |f_{\mathrm{RF}} - f_{\mathrm{LO}}|$). Mixers typically have a specified minimum LO power below which the frequency-conversion performance degrades drastically. At millimeter-wave frequencies, it may be difficult to meet these power requirements with an integrated oscillator. Subharmonic mixers (SHMs) offer an alternative to fundamental mixers in that the LO frequency is at some integer fraction $1/n$ of the fundamental LO frequency (i.e., $f_{\mathrm{IF}} = |f_{\mathrm{RF}} - n \cdot f_{\mathrm{LO}}|$). The benefit of this approach is that it allows the use of a LO at a relatively low frequency at which the output power and phase noise performance may be superior to that which is available at the fundamental frequency. This technique has been successfully implemented in many millimeter-wave mixer applications [2]–[6].

The most widely implemented SHM topology is the antiparallel diode configuration [7]. This consists of a pair of diodes in parallel with polarity reversed relative to one another. The advantage of this configuration is that the diode pair conducts on both the positive and negative portions of the LO cycle, resulting in an inherent 2× multiplication of the LO frequency. Therefore, ideally, the only frequency components present in the LO switching waveform are multiples of the second LO harmonic. This suppresses the fundamental mixing response, improving conversion to the subharmonic IF products.

The motivation of this research is the implementation of a 60-GHz monolithic-microwave integrated-circuit (MMIC) SHM in finite ground coplanar (FGC) waveguide technology. This transmission-line topology has several advantages for MMIC implementation [8]. These advantages include low dispersion, low line attenuation, lower radiation loss for odd-mode operation, and flexibility in designing line dimensions for a particular characteristic impedance (i.e., characteristic impedance is largely unaffected by substrate thickness) [9]. The coplanar ground planes also obviate the need for backside ground connections, simplifying processing and design by eliminating the dependence on vias for ground connections, as seen in microstrip.

II. FGC Waveguide Design

FGC line (Fig. 1) is a coplanar waveguide (CPW) variant with truncated ground plane widths to avoid the excitation of a parallel-plate waveguide mode between the CPW ground plane and backside metal plane [8], [9]. If the ground planes are made narrow enough such that the overall structure width ($w + 2g + 2W_g$, see Fig. 1) is less than a quarter of a dielectric wavelength ($\lambda_d/4$) in the substrate at the highest frequency of interest, excitation of the parallel-plate waveguide mode may be avoided without the use of vias.

Simulations were conducted using Zeland's IE3D[1] in order to determine the optimum FGC dimensions for a 50-Ω characteristic impedance on the given substrate. While advanced coplanar models are becoming available within microwave computer-aided design (CAD) software environments, such models were not available to the authors at the time this study was performed, necessitating this standalone electromagnetic (EM) analysis. The lines were simulated as 4.5-μm-thick

Manuscript received August 6, 2001; revised October 20, 2001.

M. W. Chapman was with the Bradley Department of Electrical and Computer Engineering, Virginia Polytechnic Institute and State University, Blacksburg, VA 24061 USA. He is now with the Alfred Mann Foundation, Valencia, CA 91355-4856 USA (e-mail: mwchap@aemf.org).

S. Raman is with the Bradley Department of Electrical and Computer Engineering, Virginia Polytechnic Institute and State University, Blacksburg, VA 24061 USA (e-mail: sraman@vt.edu).

Digital Object Identifier 10.1109/TMTT.2002.804638

[1]*IE3D*, rel. 5, Zeland Software, Inc., Fremont, CA, 1998.

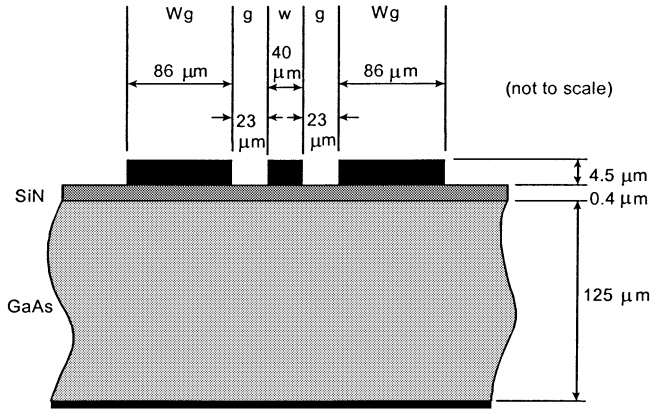

Fig. 1. FGC line topology and standard 50-Ω dimensions.

gold conductors on a 125-μm-thick GaAs ($\varepsilon_r = 12.9$, $\tan\delta = 0.006$) substrate corresponding to the available process technology (M/A-COM, Roanoke, VA, MSAG-5). The process also includes a 0.4-μm-thick SiN ($\varepsilon_r = 7.0$, $\tan\delta = 0.002$) passivation layer (as shown in Fig. 1), which is accounted for in the simulations. The center conductor width is practically limited by line attenuation, dispersion, and the requirement to maintain a total structure width less than $\lambda_d/4$ to avoid parasitic mode excitations. If the line is too narrow, the line attenuation may become prohibitively high. At greater linewidths, dispersion may arise, indicated by a varying effective dielectric constant over frequency. The ground-plane widths (W_g) were set to be equal to the overall slot width $(w + 2g)$.

The simulated effective dielectric constant and line attenuation for various center conductor widths are shown in Fig. 2(a) and (b), respectively. These graphs indicate that a center conductor width of 40 μm offers an acceptable combination of low line attenuation and low dispersion (indicated by the flatness of the $\varepsilon_{\rm eff}$ plot). The FGC dimensions shown in Fig. 1 reflect the standard 50-Ω transmission-line dimensions for the given substrate as simulated. These dimensions were subsequently used as the standard FGC transmission-line dimensions throughout development of the mixer.

III. Mixer Design and Simulation

4× SHMs were designed and simulated using the HP (now Agilent) EEsof Series IV simulation software.[2] The simulated mixer schematic is shown in Fig. 3. These simulations were conducted with ideal distributed transmission-line elements and the standard Libra p-n diode model. The diode model parameters were provided by the foundry (M/A-COM, Roanoke, VA) and are shown in Table I.

For best mixer performance, it is important that the full LO voltage be dropped across the diode pair. The $\lambda_g/4@f_{\rm LO}$ open-circuit stub terminates the diode pair in a short circuit at the side opposite the LO port. Similarly, a $\lambda_g@f_{\rm RF}$ short-circuit stub on the opposite side from the RF port provides a short circuit at RF. For a 4× SHM, the RF is approximately equal to four times the LO frequency. Therefore, the $\lambda_g@f_{\rm RF}$ stub is approximately

[2]*HP EESof Communications Design Suite* ver. 6.6, Hewlett-Packard Company, Santa Clara, CA, 1997.

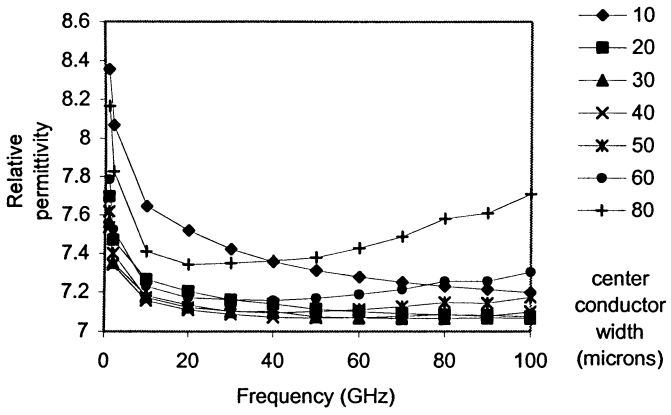

(a)

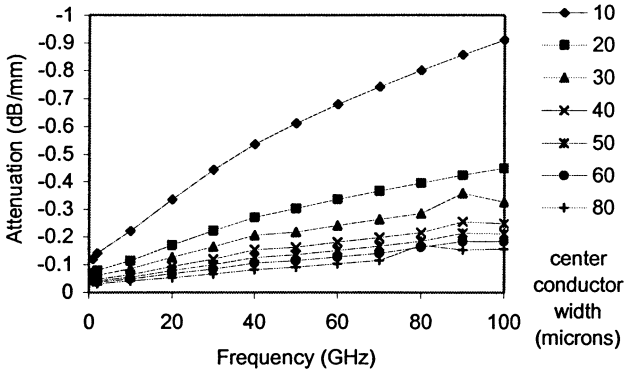

(b)

Fig. 2. Simulated FGC line characteristic for various center conductor widths. (a) Effective permittivity. (b) Line attenuation.

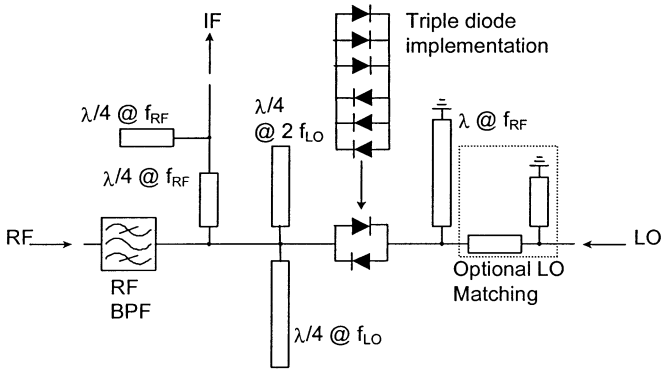

Fig. 3. Schematic of the 4× SHM design.

equal to $\lambda_g/4$ at the LO frequency. This presents an open circuit at this frequency, allowing the LO signal to pass undisturbed.

The IF port is coupled to the diodes via a $\lambda_g/4@f_{\rm RF}$ transmission line. On the IF port side of the transmission line is a shunt $\lambda_g/4@f_{\rm RF}$ open-circuit stub. The purpose of this network is to present an open circuit to the RF signal so that the IF port does not degrade conversion loss by loading the RF signal. The components used in this network are electrically small enough at the IF to be essentially transparent at that frequency. The RF bandpass filter (BPF) indicated in the schematic serves a similar purpose. This filter passes the RF frequencies, but presents an open circuit at IF frequencies so the IF signal is not loaded by the impedance of the RF port. This filter was implemented

TABLE I
M/A-COM MSAG-5 SCHOTTKY MIXER DIODE PARAMETERS

Saturation current (pA)	Series resistance (Ω)	Ideality factor	Carrier lifetime (ps)	Junction capacitance (fF)	Built-in voltage (V)	Bandgap voltage (eV)	Reverse breakdown voltage (V)	Breakdown current (mA)
0.2	17.6	1.25	1.0	13.5	0.73	1.43	-7	200

with an FGC series open-circuit stub, which was modeled with an equivalent lumped *L-C* circuit based on IE3D modeling for Libra simulations [6].

The diode pair indicated in the schematic was implemented using two variations of the antiparallel Schottky diode configuration. In the first configuration, the diode pair is connected as shown in the schematic. In the second variant, however, three parallel Schottky diodes (layout unit cells) are substituted for each diode indicated in the schematic. This was done in an effort to reduce the effects of diode series resistance (R_s) on mixer conversion loss; R_s is known to be a major contributor to diode mixer conversion loss. The parallel combination of three diodes divides the effective R_s of the structure by an approximate factor of three.

Since this is a 4× SHM, it is desirable to suppress other undesired subharmonic conversion products. These products arise from conversion of RF power to output frequencies such as $f_{\rm RF}-2f_{\rm LO}$ and $6f_{\rm LO}-f_{\rm RF}$. These mixing products represent a loss mechanism to the 4× subharmonic conversion product by stealing converted RF power that would otherwise be converted to the 4× subharmonic IF. Since the RF is approximately equal to $4f_{\rm LO}$, the $f_{\rm RF}-2f_{\rm LO}$ product falls at approximately $2f_{\rm LO}$. Therefore, the $\lambda_g/4@2f_{\rm LO}$ stub is included at the side of the diode pair from which the IF is extracted. Similarly, the $6f_{\rm LO}-f_{\rm RF}$ conversion product also falls at approximately $2f_{\rm LO}$ and is, therefore, suppressed by the presence of the $\lambda_g/4@2f_{\rm LO}$ stub. Fig. 4 shows the simulated conversion loss of the desired mixing product $(f_{\rm RF}-4f_{\rm LO})$ compared to that of the unwanted mixing products ($f_{\rm RF}-2f_{\rm LO}$ and $6f_{\rm LO}-f_{\rm RF}$). Fig. 4(a) shows that without the $\lambda_g/4@2f_{\rm LO}$ stub, the undesired $f_{\rm RF}-2f_{\rm LO}$ output product is dominant, actually having better conversion loss than the desired 4× subharmonic conversion product. Fig. 4(b) shows the simulated conversion loss of the circuit after the addition of the $\lambda_g/4@2f_{\rm LO}$ stub. It can be seen that, at the optimal LO drive levels, the $f_{\rm RF}-2f_{\rm LO}$ conversion loss is degraded by 15 dB. The result is an improved conversion loss for the desired IF product $f_{\rm RF}-4f_{\rm LO}$. In this particular case, the $6f_{\rm LO}-f_{\rm RF}$ conversion product does not significantly affect mixer performance since its conversion loss is approximately 15 dB greater than the RF-$4f_{\rm LO}$ product with or without the $2f_{\rm LO}$ stub. The difference in mixer performance with and without the $2f_{\rm LO}$ suppression stub is plotted versus frequency in Fig. 5.

An optional LO matching network was included in some mixer simulations in an effort to reduce the LO power required for optimal mixer conversion loss. This network consists of a series delay line followed by a shunt short-circuit stub. Fig. 6 shows the simulated impedance presented to the LO port before and after the addition of the matching network. It is evident from this graph that the port impedance has a capacitive reactance prior to the addition of the matching network. The

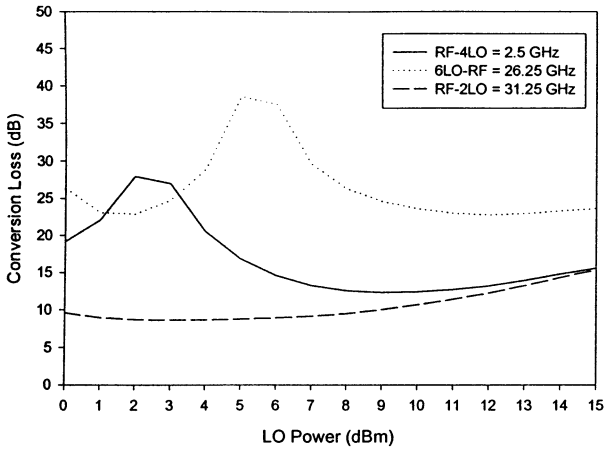

(a)

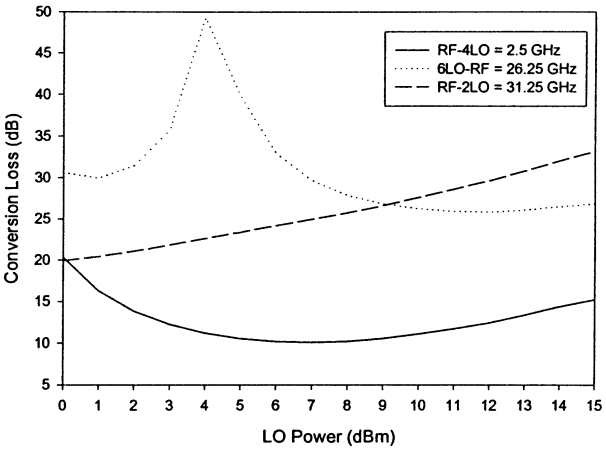

(b)

Fig. 4. Simulated conversion loss versus LO power of various mixing products (triple-diode mixer $\rm RF = 60$ GHz). (a) No $2f_{\rm LO}$ suppression stub. (b) With $2f_{\rm LO}$ suppression stub.

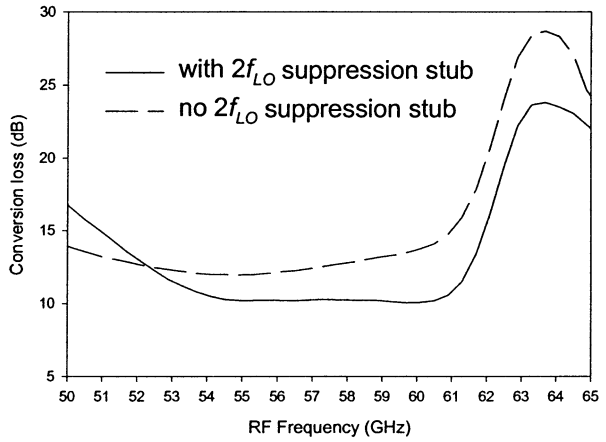

Fig. 5. Simulated upper sideband (USB) conversion loss versus frequency for various mixing products (triple-diode mixer with and without $2f_{\rm LO}$ stub, LO power = 7 dBm).

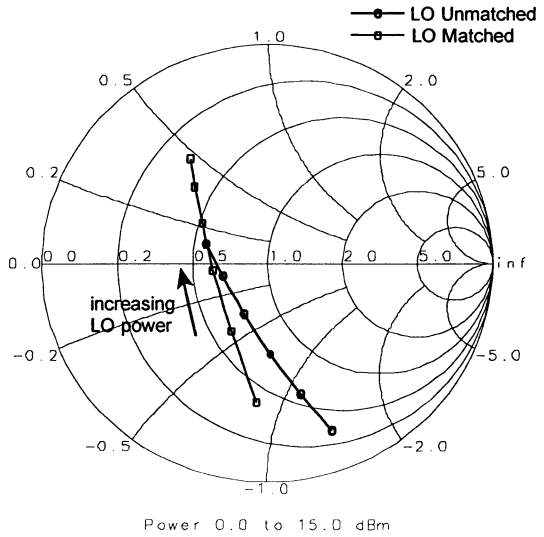

Fig. 6. Simulated LO input impedance (triple-diode mixer).

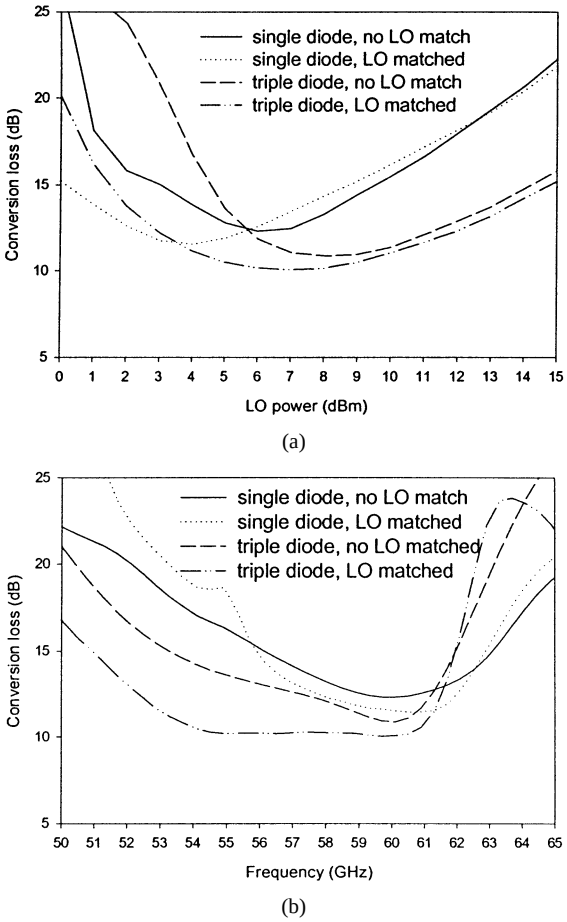

Fig. 7. Simulated conversion loss of various mixer configurations: (a) versus LO power at $f_{\mathrm{RF}} = 60$ GHz and (b) versus RF frequency at respective LO power levels for minimum conversion loss, as shown in (a) for $f_{\mathrm{RF}} = 60$ GHz.

short-circuit matching stub is inductive at the LO frequency, providing an approximate conjugate match to the capacitive reactance presented by the diodes. The length of this stub was determined by iterative tuning for optimum mixer conversion loss, not necessarily to provide an exact conjugate match. In a comparison of the matched and unmatched input impedances,

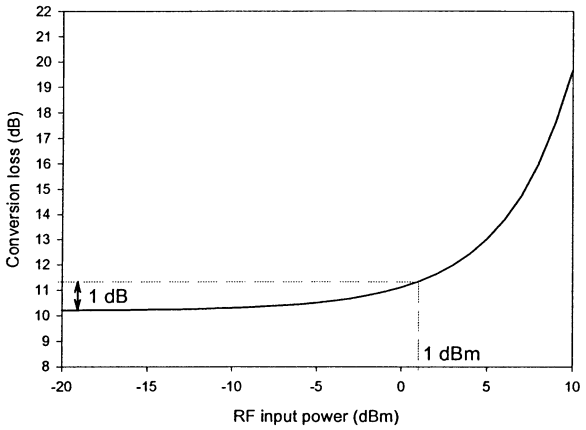

Fig. 8. Simulated 1-dB compression point of triple-diode mixer with LO matching ($f_{\mathrm{RF}} = 60$ GHz, LO power $P_{\mathrm{LO}} = 7$ dBm).

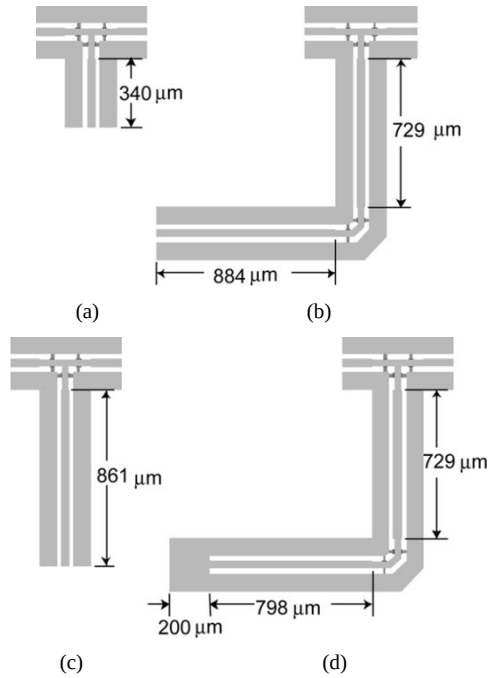

Fig. 9. FGC distributed stub layout dimensions. (a) Open-circuit $\lambda_g/4@f_{\mathrm{RF}}$. (b) Open-circuit $\lambda_g/4@f_{\mathrm{LO}}$. (c) Open-circuit $\lambda_g/4@2f_{\mathrm{LO}}$. (d) Short-circuit $\lambda_g@f_{\mathrm{RF}}$.

the two are fairly similar. A given impedance point, however, occurs at a noticeably lower LO power for the matched case than for the unmatched case. This behavior is mirrored in the simulated conversion loss performance.

The simulated conversion loss data for the four mixer variations are shown in Fig. 7(a) and (b). The effect of the matching networks can be seen in Fig. 7(a). In the case of the single-diode mixer, the optimum LO drive level shifts from between 6–7 dBm to between 3–4 dBm with the addition of the LO matching networks. A similar shift is shown for the triple-diode mixer, for which the optimum LO power shifts from 7–9 to 6–8 dBm. In both cases, the LO matching networks result in a slight improvement in conversion loss. The best simulated conversion loss shown by all variants is 10. 0 dBm for the triple-diode mixer with LO matching at an RF of 60 GHz with an LO power of 7 dBm at 14.375 GHz.

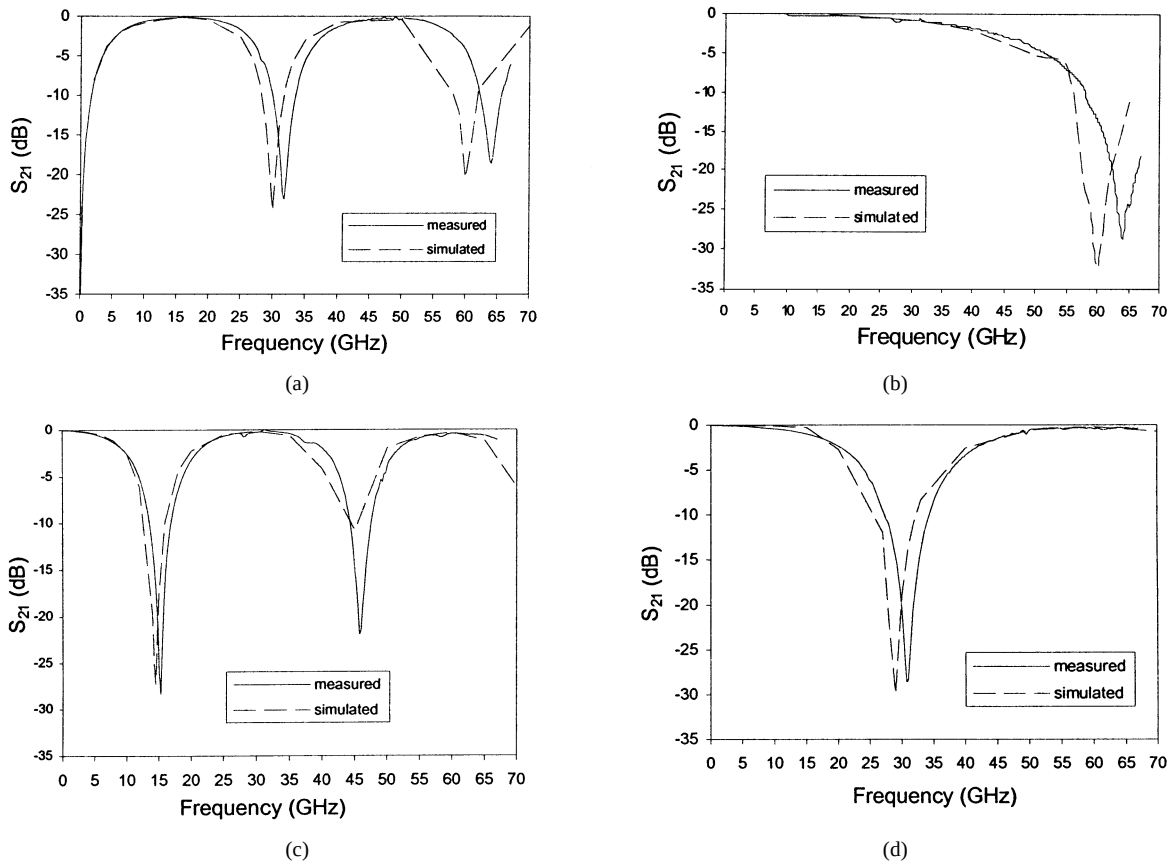

Fig. 10. Simulated and measured transmission coefficient of distributed tuning elements. (a) Open-circuit $\lambda_g/4@f_{\rm RF}$. (b) Short-circuit $\lambda_g@f_{\rm RF}$. (c) Open-circuit $\lambda_g/4@f_{\rm LO}$. (d) Open-circuit $\lambda_g/4@2f_{\rm LO}$.

Linearity is of particular concern with SHMs, which are known to display higher distortion than their fundamental counterparts [7]. Fig. 8 shows that the triple-diode mixer with LO matching has a simulated 1-dB input compression point of 1 dBm. This is somewhat low compared to other passive mixers. This problem could be compounded by the fact that, although a high preceding low-noise amplifier (LNA) gain would overcome the mixer conversion loss, it would exacerbate the signal distortion in the mixer. This is a critical consideration in determining whether this mixer topology is suitable for satisfying the system performance requirements.

IV. FGC Stub Implementation and Measurements

In order to duplicate the simulated mixer performance in a fabricated MMIC mixer, it was necessary to implement the distributed circuit elements in a practically realizable FGC topology. The FGC dimensions in Section II were, therefore, used as a starting point for the distributed stub elements required for the mixer design in Section III. Discontinuities such as bends and tee-junctions must be considered in stub design, as well as open-end capacitance in open-circuit FGC stubs. Therefore, circuit dimensions were selected by simulating the physical structures in IE3D and iteratively tuning the stub length to achieve resonance at the desired frequencies. This process was used to determine the dimensions of the shunt tuning stubs and the series open-circuit stub used for the RF port filter.

A. Shunt Stubs

The physical structures simulated during stub design are shown in Fig. 9. The FGC ground planes are equalized at discontinuities (to suppress excitation of the unwanted even or "slotline" mode) using dielectric-supported center-conductor crossovers available in the given process technology. The crossovers are compensated with narrower (inductive) center conductor widths at the junctions. A comparison of the fabricated and simulated stub performance is shown in Fig. 10. All stubs were found to resonate approximately 7% above their intended resonant frequency. This is attributed to the fact that two-dimensional (infinitesimal thickness) conductors of finite conductivity were used in simulating the distributed elements. The resonant frequency of the FGC lines is dependent on the effective permittivity of the FGC lines $(\varepsilon_{\rm eff})$. This model neglects the coupling between the sidewalls of the FGC center conductor and ground planes, which would otherwise tend to increase the field lines existing above the GaAs substrate. The effect of this is to reduce the effective dielectric constant $(\varepsilon_{\rm eff})$, resulting in a longer guided wavelength for a given frequency. Therefore, a given physical line length will be electrically shorter and resonate at a higher frequency. Fig. 11 shows the measured FGC transmission-line parameters, extracted from on-wafer thru reflect line (TRL) calibration standards using the National Institute of Standards and Technology (NIST) MultiCal program [10]. The measured $\varepsilon_{\rm eff}$ is shown to be 6.1, compared to the simulated value of 7.1.

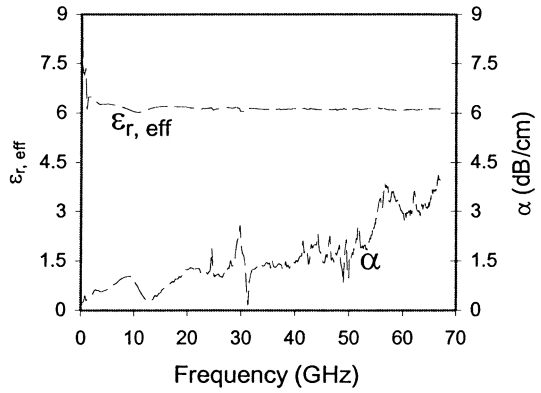

Fig. 11. Measured FGC transmission-line parameters, effective dielectric constant $(\varepsilon_{r,\mathrm{eff}})$, and line attenuation (α) for 50-Ω-line dimensions $w = 40\ \mu$m, $g = 23\ \mu$m, and $W_g = 86\ \mu$m.

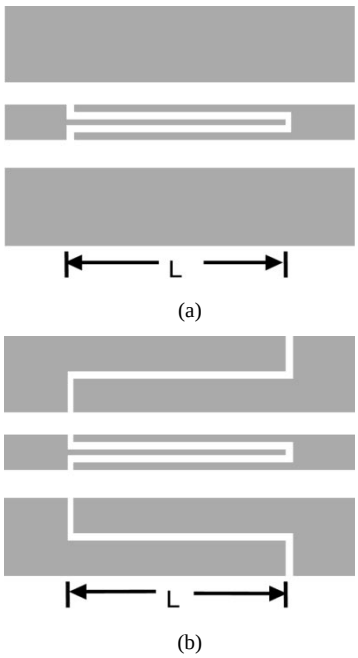

(a)

(b)

Fig. 12. Series-stub filter layouts: (a) in center conductor and (b) in center *and* ground conductors ($L = 470\ \mu$m). The lines have the same conductor dimensions as the standard 50-Ω lines discussed above. The *gaps* in the center conductors and ground planes are chosen to be 8 μm.

B. Series Stubs

Series $\lambda_g/4@f_{\mathrm{RF}}$ open-circuit stubs were used to implement the BPF required for mixer operation, as described in Section III. An interesting possibility in FGC lines is to place series stubs in the ground plane [8]. In this case, it would be advantageous to increase the rejection of the BPF at the LO and IF frequencies. If a series stub were to be implemented in both the center conductor and ground planes, it would effectively cascade the out-of-band rejection of the center and ground conductor stubs in series. A layout of open-circuit series stubs is shown in Fig. 12 with stubs in the center conductor [see Fig. 12(a)] and in both the center conductor and ground planes [see Fig. 12(b)], where L is equal to $\lambda_g/4@f_{\mathrm{RF}}$ (470 μm). The lines have the same conductor dimensions as the standard 50-Ω lines discussed above. The *gaps* in the center conductors and ground planes are chosen to be 8 μm. A plot of the measured transmission coefficients is shown in Fig. 13. This demonstrates that the inclusion of an open-circuit stub in the ground plane improves filter rejection at lower frequencies. It should be noted, however, that since this introduces an open circuit in the ground conductor at low frequencies, the ground planes at either port of the filter must be electrically isolated to achieve optimum out-of-band rejection. Otherwise, any other existing system ground paths, such as dc supply grounds, could serve as an alternate return path for the low-frequency ground signal, circumventing any rejection achieved by the open-circuit stubs.

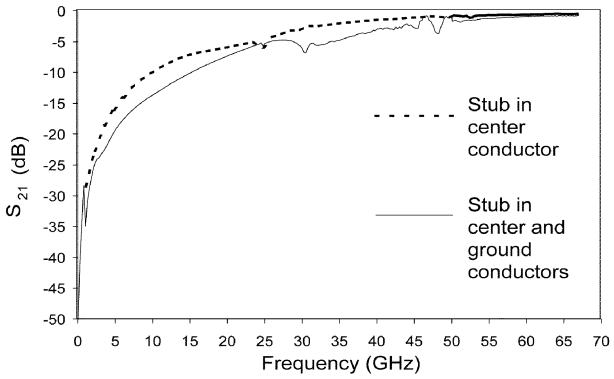

Fig. 13. Series-stub filter measured transmission coefficients.

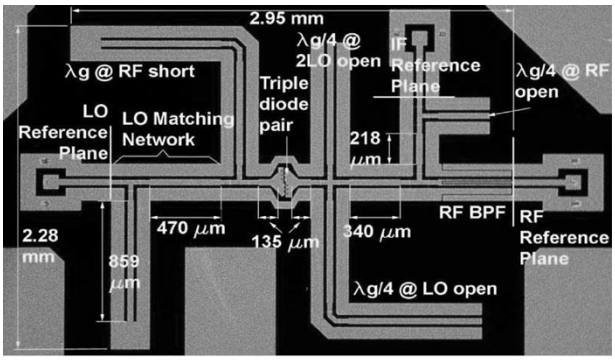

Fig. 14. Photograph of triple-diode mixer with LO matching.

V. Mixer Implementation and Measurements

The mixer circuits designed in Section IV were implemented in the M/A-COM MSAG 5 process. A photograph of the fabricated triple-diode mixer with LO matching is shown in Fig. 14. Wafer probe pads and FGC transitions are located at the respective reference planes of the IF, RF, and LO ports for measurement purposes. The overall area for the largest mixer layout (triple diode mixer with LO matching) excluding the probe pads is approximately 2.3 mm × 3.0 mm. The test setup for conversion loss is shown in Fig. 15. This setup may be easily modified for LO–RF and LO–IF isolation measurements by using the spectrum analyzer to monitor LO power at the RF and IF ports. The losses of all cables, probes, etc. were calibrated out up to the reference planes indicated on the mixer die photograph.

The measured USB conversion loss versus RF frequency is shown for the various mixer configurations in Fig. 16. The simulated data suggest that the mixers display optimal conversion

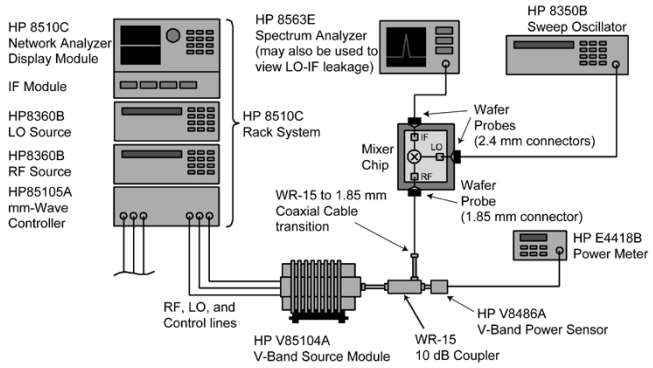

Fig. 15. Mixer conversion-loss test setup.

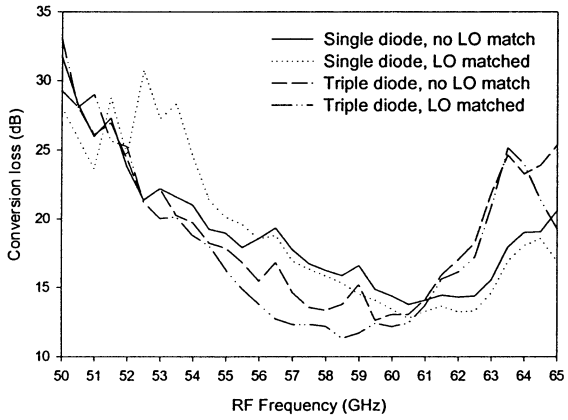

Fig. 16. Measured mixer USB conversion loss versus RF frequency ($f_{\rm IF} = 2.5$ GHz), optimum LO drive level at each frequency.

loss at the frequency to which the stub elements are tuned. If this holds true for the actual fabricated mixers, the measured optimal conversion loss should occur at an RF of 64 GHz. Fig. 16 shows that this is not the case; the single-diode mixers are optimally tuned between 60.5–62.5 GHz and the triple-diode mixer are tuned between 58.5–60.5 GHz. It is believed that this is due to parasitic capacitance in parallel with the diodes in the mixer layout causing an in-band loss increase over the band. This capacitance data was not available for diode modeling in Libra. Its effect is more pronounced in the case of the triple-diode mixer because the layout must be physically wider due to the three adjacent diodes, resulting in increased parasitic capacitance. This explains why the increase in conversion loss is more drastic for the triple-diode mixers and begins to take effect at a lower frequency. An LO power sweep is shown in Fig. 17. The benefit of the LO matching network is demonstrated in an improvement in conversion loss and a reduction in required LO power. For the case of the triple-diode mixer, the additional matching network allows the mixer to operate with better than 13-dB conversion loss at LO powers as low as 2.5 dBm.

Isolation measurements were made for the LO–IF and LO–RF signal paths. For the mixer variant with the best conversion loss, the triple-diode mixer with LO matching, the LO–IF isolation is as low as 17 dB, shown in Fig. 18(a). This is due to the fact that the stubs are mistuned to an RF of 64 GHz, corresponding to an LO of 15.5 GHz. LO isolation at all ports is largely determined by the rejection provided

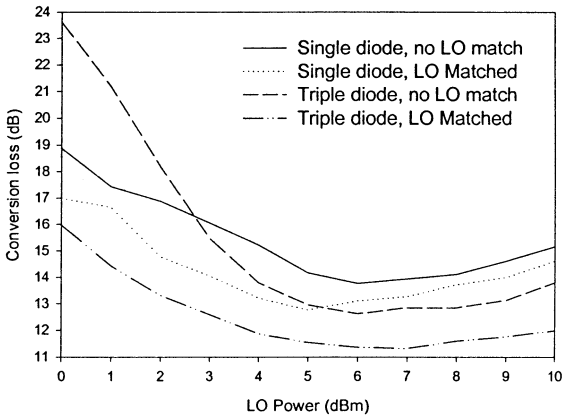

Fig. 17. Measured mixer USB conversion loss versus LO power ($f_{\rm RF} = 60$ GHz, $f_{\rm IF} = 2.5$ GHz).

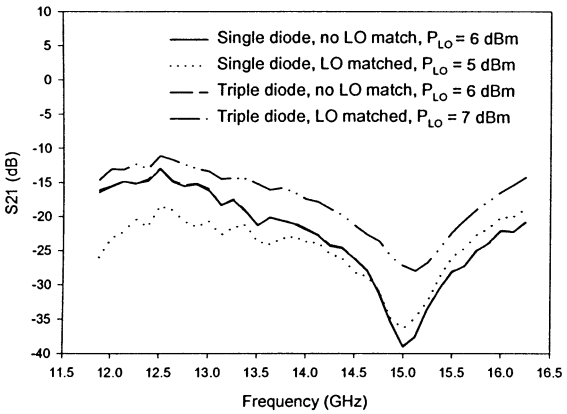

(a)

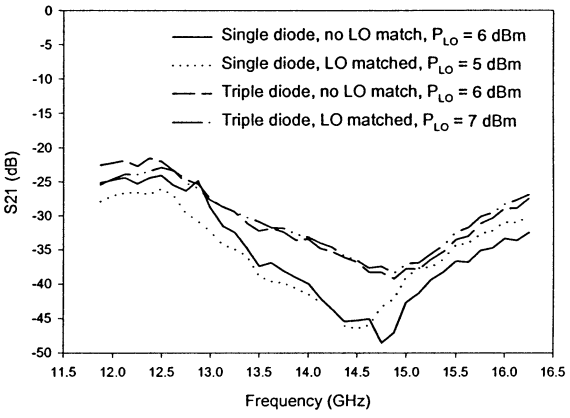

(b)

Fig. 18. Isolation versus frequency at optimum LO drive levels. (a) LO–IF. (b) LO–RF.

by the $\lambda_g/4@f_{\rm LO}$ open-circuit stub. The worst-case LO–IF isolation occurs at an RF of 58.5 GHz ($f_{\rm LO} = 14$ GHz for USB mixing at $f_{\rm IF} = 2.5$ GHz), well outside the optimum rejection provided by this stub. The LO–RF isolation [see Fig. 18(b)], which is also dominated by the rejection of the $\lambda_g/4@f_{\rm LO}$ open-circuit stub, is 33 dB in the worst case for the intended frequencies of operation. Both LO–IF and LO–RF isolation would be improved by retuning the resonant stubs for the correct operating frequencies in a subsequent design iteration.

TABLE II
MIXER PERFORMANCE COMPARED TO OTHER RECENTLY REPORTED 60-GHz INTEGRATED MIXERS

Mixer Topology	Active or Passive	LO mixing harmonic	Max. Conversion Gain (dB)	LO Power (dBm)	Reference
Image reject MESFET	Active	Fund.	1	5	[15]
Source injected FET	Active	Fund.	0	7	[16]
Gate injected HEMT	Active	Fund.	5	4.5	[17]
Drain-injected HEMT	Active	Fund.	3.7	10	[18]
Resistive HEMT	Passive	Fund.	-7.7	5	[18]
Dual-gate HFET	Active	Fund.	-5	5	[19]
Antiparallel diode	Passive	2^{nd}	-14	-3	[20]
Antiparallel diode	Passive	2^{nd}	-13		[14]
Antiparallel diode	Passive	2^{nd}	-12	8	[13]
Antiparallel diode	Passive	4^{th}	-11.3	7	This work

An I–V measurement was made for the fabricated Schottky diodes in order to extract an approximate value for R_s. The extracted value was 20.0 Ω compared to the foundry specification of 17.6 Ω. This partially accounts for the degradation in measured conversion loss compared to the simulated values.

Mixer linearity could not be measured due to the lack of sufficient available RF power to perform $P_{1\text{dB}}$ testing or a second 60-GHz source for third-order intercept point (IP3) testing. The noise figure of the mixer was not measured due to lack of millimeter-wave noise test capabilities, although it is expected that the noise figure will be approximately equal to the conversion loss as is generally the case with passive mixers with reasonably low LO–IF isolation.

VI. CONCLUSIONS

A high-performance 60-GHz mixer has been fabricated in a uniplanar (FGC) GaAs MMIC technology. The best performance is displayed by the triple-Schottky-diode mixer with an LO matching network. This circuit displayed an 11.3-dB USB conversion loss at an RF of 58.5 GHz and IF of 2.5 GHz. The size of this circuit is approximately 2.3 mm × 3 mm excluding wafer probe pads. The USB operating range for the RF has been defined as 58.5–60.5 GHz and the IF range has been defined as 1.5–2.5 GHz. Less than 13.3-dB conversion loss is achieved over this range with an LO power of 3–10 dBm.

Two other recently reported 60-GHz antiparallel diode 2× SHMs have shown conversion losses of 12 [11] and 13 dB [12]. These and other recently reported 60-GHz mixer results are summarized in Table II. Typically, a 3-dB conversion-loss degradation is observed when going from 2× to 4× subharmonic mixing. With these reported results as a benchmark, a conversion loss under 13.3 dB over the defined range of operating frequencies represents excellent conversion loss for a 4× SHM.

ACKNOWLEDGMENT

The authors thank B. Schmitz, M/A-COM, Roanoke, VA, A. Peroni, M/A-COM, J. Allen, M/A-COM, B. Sloane, M/A-COM, J. Dilley, M/A-COM, and M. Balzan, M/A-COM, for fabrication of the mixer designs in this study. Author S. Raman thanks Prof. G. Rebeiz, The University of Michigan at Ann Arbor, for support during initial development of the mixer concept, under funding from the Naval Surface Warfare Center (NSWC), Dahlgren, VA, and the Army Research Office under Contract DAAH04-96-1-0348. The Antenna Group, Virginia Polytechnic Institute and State University, Blacksburg, provided valuable test equipment resources.

REFERENCES

[1] F. Giannetti, M. Luise, and R. Reggiannini, "Mobile and personal communications in the 60 GHz band: A survey," *Wireless Pers. Commun.*, vol. 10, pp. 207–243, 1999.

[2] B. Kormanyos, C. Ling, and G. Rebeiz, "A planar wideband millimeter-wave subharmonic receiver," in *IEEE MTT-S Int. Microwave Symp. Dig.*, Boston, MA, June 10–14, 1991, pp. 213–216.

[3] D. Blackwell, H. G. Henry, J. E. Degenford, and M. Cohn, "94 GHz subharmonically pumped MMIC mixer," in *IEEE MTT-S Int. Microwave Symp. Dig.*, Boston, MA, June 10–14, 1991, pp. 1037–1039.

[4] H. Zirath, I. Angelov, and N. Rorsman, "A millimeter-wave subharmonically pumped resistive mixer based on a heterostructure field effect transistor technology," in *IEEE MTT-S Int. Microwave Symp. Dig.*, Albuquerque, NM, June 1–5, 1992, pp. 599–602.

[5] A. Madjar and M. Musia, "A ×4 low loss microstrip 38.5 to 40 GHz subharmonic mixer," *Microwave J.*, pp. 107–110, June 1994.

[6] S. Raman, F. Rucky, and G. Rebeiz, "A high-performance W-band uniplanar subharmonic mixer," *IEEE Trans. Microwave Theory Tech.*, vol. 45, pp. 955–962, June 1997.

[7] S. Maas, *Microwave Mixers*. Norwood, MA: Artech House, 1993.

[8] G. Ponchak and L. Katehi, "Finite ground coplanar (FGC) waveguide: A better transmission line for microwave circuits," *Adv. Microelectron.*, pp. 15–18, May/June 1998.

[9] R. Jackson, "Considerations in the use of coplanar waveguide for millimeter-wave integrated circuits," *IEEE Trans. Microwave Theory Tech.*, vol. MTT-34, pp. 1450–1456, Dec. 1986.

[10] R. B. Marks and D. F. Williams, *Multical v1.00*. Boulder, CO: NIST, 1995.

[11] Y. Kok, P. Huang, H. Wang, B. Allen, R. Lai, M. Sholley, T. Gaier, and I. Mehdi, "120 and 60 GHz monolithic InP-based HEMT diode mixer," in *IEEE MTT-S Int. Microwave Symp. Dig.*, Baltimore, MD, June 7–12, 1998, pp. 1723–1726.

[12] C. Verver, T. Laneve, and M. Stubbs, "Design of a 60 GHz subharmonic mixer MMIC," in *Proc. Antenna Technol. and Appl. Electromagn. Symp.*, Ottawa, ON, Canada, Aug. 9–12, 1998, pp. 65–68.

[13] K. Nishikawa, S. Sugitani, K. Inoue, K. Kamogawa, T. Tokumitsu, I. Toyoda, and M. Tanaka, "A compact V-band 3D MMIC single-chip downconverter using photosensitive BCB dielectric film," in *IEEE MTT-S Int. Microwave Symp. Dig.*, Anaheim, CA, June 12–19, 1999, pp. 131–134.

[14] M. Mahidian, L. Desclos, K. Maruhashi, K. Onda, and M. Kuzuhara, "60-GHz monolithic down and upconverters utilizing a source-injection concept," *IEEE Trans. Microwave Theory Tech.*, vol. 46, pp. 1003–1006, July 1998.

[15] M. Schefer, U. Lott, H. Benedickter, H. Meier, W. Patrick, and W. Bächtold, "Active, monolithically integrated coplanar V-band mixer," in *IEEE MTT-S Int. Microwave Symp. Dig.*, Denver, CO, July 1997, pp. 1043–1046.

[16] T. Kashiwa, T. Katoh, T. Ishida, T. Ishikawa, and Y. Nakayama, "A V-band drain injected/resistive dual-mode monolithic mixer," in *IEEE GaAs IC Symp. Dig.*, Monterey, CA, Oct. 17–19, 1999, pp. 117–120.

[17] R. Allam, C. Kolanowski, D. Langrez, P. Bourne, J. C. De Jaeger, Y. Crosnier, and G. Salmer, "60 GHz MMIC mixer using a dual-gate PM HEMT," in *IEEE Proc. URSI Int. Signals, Syst., and Electron. Symp.*, San Francisco, CA, Aug. 1999, pp. 171–174.

[18] J. Mizoe, T. Matsumura, K. Unosawa, Y. Akiba, K. Nagai, H. Sato, T. Saryo, and T. Inoue, "A V-band GaAs MMIC chip set on a highly reliable WSi/Au refractory gate process," in *IEEE MTT-S Int. Microwave Symp. Dig.*, Denver, CO, July 1997, pp. 247–250.

Michael W. Chapman (M'01) received the B.S.E.E. and M.S.E.E. degrees from the Virginia Polytechnic Institute and State University, Blacksburg, in 1997 and 2000, respectively, with a focus on RF and microwave circuit design.

From 1997 to 1998, he was a Member of Technical Staff with Nokia Mobile Phones, San Diego, CA. He is currently an RF Engineer with the Alfred Mann Foundation, Valencia, CA, where he is involved with transceivers for biomedical applications.

Sanjay Raman (S'84–M'98) was born on April 25, 1966, in Nottingham, U.K. He received the B.E.E. degree in electrical engineering from the Georgia Institute of Technology, Atlanta, in 1987, and the M.S.E.E. and Ph.D. degrees in electrical engineering from The University of Michigan at Ann Arbor, in 1993 and 1997, respectively. His doctoral research concerned novel millimeter-wave integrated antennas and electronics.

From 1987 to 1992, he served as a nuclear trained submarine officer with the U.S. Navy. In January 1998, he joined the faculty of the Bradley Department of Electrical and Computer Engineering, Virginia Polytechnic Institute and State University, Blacksburg, where he is an Assistant Professor. He has established the Wireless Microsystems Laboratory to explore enabling ideas and technologies for integrated microsystems, in particular, microsystems that are connected to the information infrastructure via wireless communications links. His research interests include RF/microwave/millimeter-wave integrated circuits and antennas, integrated wireless communications and sensor microsystems, high-speed/mixed-signal integrated circuits, interconnects and packaging, RF microelectromechanical/nanoelectromechanical system (MEMS/NEMS) and MEMS sensors, micromachining, and solid-state technology.

Dr. Raman was the recipient of the Presidential Early Career Award for Scientists and Engineers (PECASE) (1999), Virginia Tech College of Engineering Outstanding New Assistant Professor Award (2000), First Place IEEE Microwave Theory and Techniques Society (IEEE MTT-S) International Microwave Symposium (IMS) Student Paper Competition (1996), Armed Forces Communications and Electronics Association (AFCEA) Postgraduate Fellowship (1996–1997), and IEEE Antennas and Propagation Society (IEEE AP-S) International Symposium First Place Student Paper Competition (1995).